Scheider, I.; Rajendran, M.; Banerjee, A.:

Comparison of different stress-state dependent cohesive zone models applied to thin-walled structures

In: Engineering Fracture Mechanics (2010) Elsevier

DOI: 10.1016/j.engfracmech.2010.05.003

Comparison of Different Stress State Dependent Cohesive Zone Models Applied to Thin Walled Structures

Ingo Scheider[a], M Rajendran[b], Anuradha Banerjee[b]

[a] *GKSS Research Centre, Institute of Materials Research Geesthacht, Germany*
[b] *IIT Madras, Dept. of Applied Mechanics, Chennai, India*

Abstract

Two stress-state dependent cohesive zone model for thin walled structures proposed previously by the authors are compared. Both models incorporate the stress-state explicitly within the traction-separation law, the first one by using basic elastic-plastic constitutive equations combined with a model parameter depending on the average triaxiality in plane stress conditions, the other one by replacing the cohesive strength and cohesive energy with triaxiality dependent functions. The respective parameters for both models are identified, and then they are applied to several notched and precracked specimens. It is shown that in contrast to cohesive models with constant parameters, good predictions can be achieved with both constraint dependent models for all structures.

Key words: Cohesive zone model, ductile fracture, triaxiality, plane stress, thin-walled structures

1. Introduction

Thin walled structures are widely used in many branches of industry to save both mass and, especially in transport industries, energy consumption. However, in order to ensure the structural integrity of thin-walled structures it is of significance to deve lop advanced models that are able to capture the failure mechanisms occurring in such structures. For metal sheets, in particular, two characteristic features of their failure must be taken into account: The model must be able to simulate significant stable crack extension prior to final failure, but more importantly should be

Email addresses: ingo.scheider@gkss.de (Ingo Scheider), rajendran_rec@yahoo.com (M Rajendran), anuban@iitm.ac.in (Anuradha Banerjee)

sensitive to the significant differences in the stress state of precracked or initially uncracked sheets [1, 2].

In the cohesive zone framework, the stress-state dependence of the fracture process under plane strain has been the subject of investigations during the last decade. Using porous plasticity damage mechanics on unit cells, triaxiality dependent traction-separation laws (TSLs) have been developed and successfully applied to various geometries [3, 4, 5]. However, corresponding analyses are difficult to perform using void growth models as they have difficulties in dealing with low triaxiality of thin-walled structures, see e.g. [6]. As a workaround one can also identify the triaxiality dependence by fitting the results of crack extension simulations to experiments on specimens with varying triaxiality, e.g. structures with and without cracks. Afterwards this dependence might be expr essed by an analytical function for the range investigated.

Another possibility is to identify the parameters for a specific range of triaxiality as mentioned above, and then to apply the cohesive zone model with constant parameters to structures with similar constraint, i.e. uncracked structures with a low triax iality have different parameters compared to precracked structures [7]. The advantage of this method is that no explicit triaxiality dependence is needed (which is a problem for commercial finite element codes anyway), and only tests for param eter identification in the range of the structure to be analyzed have to be performed.

Cohesive zone model has been most extensively used in the prediction of failure of structures with a preexisting crack, where the error made by the assumption of constant cohesive model parameters is small, see [3].

Recently a stress-state dependent model which incorporates triaxiality explicitly has been proposed [8]. The model described therein for plane strain mode I ductile fracture is formulated by using basic elastic-plastic constitutive equations combined with two stress-state independent new model parameters, which capture the triaxiality dependent failure strai n. This methodology has been extended to plane stress conditions in [9] providing a stress-state dependent cohesive model for thin-walled structures. Cohesive elements based on the proposed model were applied to predict experimental data on fracture of notched as well as precracked thin sheet fracture specimens of Aluminium Al 5083. It has been shown that the proposed model is able to closely approximate the macroscopic behaviour observed experimentally for both the notched as well as precracked sheet specimens.

In the current paper this validation is extended to more specimens in order to show that the effect of constraint can be captured by this model. In addition, a classical cohesive zone model will be applied to the same specimens with triaxiality dependent parameters cohesive strength, σ_{max}, and cohesive energy, Γ_{n0}. Due to the difficulties arising from application of porous metal plasticity model the constraint dependence is determined by adjusting the simulated curves to the experimental ones.

2. Cohesive model formulations

For the definition of the constitutive behaviour of the cohesive zone model, different approaches have been presented in the literature. Since the concept of cohesive zone modelling is assumed to be well known and numerous publications exist on this topic , only very few publications are given in the following.

For the development of the constitutive behaviour, research groups may start from a free energy potential and calculate the traction-separation law by derivation of the potential with respect to the separation, see e.g. [10]. Other groups start directly with a relation between tractions, $\mathbf{T}$ with its normal and tangential components, T_n and T_t, and separations, $\binom{\delta=\delta_n}{\delta_t}$ without explicitly checking thermodynamic consistenc y, cf. [11]. A third group uses traction-separation laws based on conventional material laws based on stress and strain, usually including elasticity and continuum damage mechanics, see e.g. [12]. In this case the interface properties are derived by either a finite height of the interface or a ficticious height in order to calculate the material separation. All of these approaches have in common that a (not necessarily constant) cohesive strength exists which is the maximum stress that can be transferred across the cohesive interface. In addition, a cohesive energy can be defined, which is the energy dissipa ted by one cohesive element upon total failure. It is calculated from the integral of cohesive stress over separation, that is for pure normal separation:

$$\Gamma_{n0} = \int_0^{\delta_{n0}} T_n d\delta_n \tag{1}$$

The critical separation, δ_{n0}, is a dependent parameter, if σ_{max} and Γ_{n0} are known. The cohesive energy may also depend on other quantities.

Theoretically, all of these models may incorporate a stress state dependence, which is needed to calculate the different structures shown later on. Under plane stress conditions one may define the stress triaxiality based on the ratio between the two in-plane principal stresses $\alpha = \sigma_I/\sigma_{II}$ as:

$$H = \frac{\sigma_{mean}}{\sigma_{mises}} = \frac{1+\alpha}{3\sqrt{\alpha^2 - \alpha + 1}} \tag{2}$$

Fig. 1 shows that the triaxiality parameter increases with increasing bi-axiality ratio up to $\alpha = 0.6$, beyond which it tends to saturate to the maximum possible value of 2/3. Compared to plane strain triaxiality, the plane stress parameter does not exhibit singular behaviour for α tending to unity. Remarkably, the lowest possible triaxiality in plane strain (0.577) and the highest possible in plane stress (0.666) are reasonably close to each other.

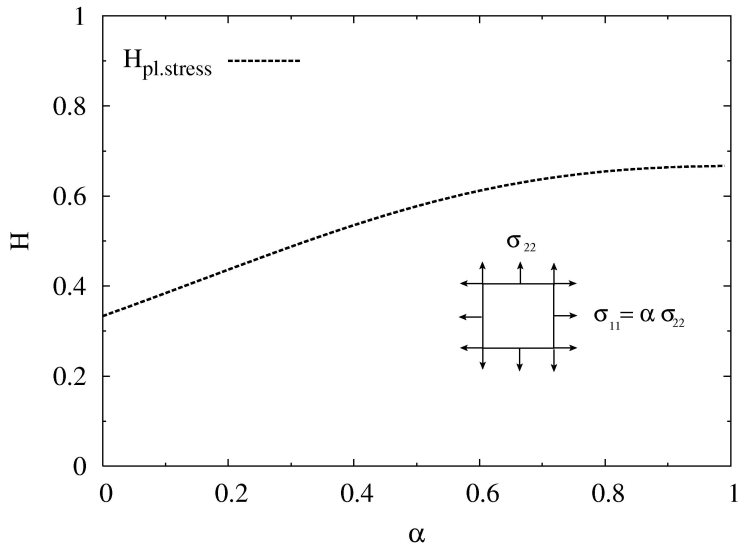

Figure 1: The dependence of triaxiality parameter on a fixed applied bi-axiality ratio, α, under conditions of plane stress.

Two approaches for the derivation of cohesive zone models are described in the following: The first one starts with a traction-separation law proposed by Scheider [13], in which the main parameters are triaxiality dependent, the other one starts with the plasticity within a finite fracture process zone and adds a damage behaviour aft er a critical state (the failure strain) depending on triaxiality [8, 9]. The first one will be called Scheider-approach, the latter Banerjee-approach in the following in order to distinguish easily between the models.

2.1. Model incorporating triaxiality dependent parameters

The traction separation law used here is one with a partly constant stress over a finite range of separation, and with a steadily differentiable shape as shown in Fig. 2(a). The corresponding equation for this graph is given by

$$T_n = \sigma_{max} \begin{cases} \left[2\left(\frac{\delta}{\delta_{n1}}\right) - \left(\frac{\delta}{\delta_{n1}}\right)^2\right] & \delta < \delta_{n1} \\ 1 & \delta_{n1} < \delta < \delta_{n2} \\ \left[2\left(\frac{\delta-\delta_{n2}}{\delta_{n0}-\delta_{n2}}\right)^3 - 3\left(\frac{\delta-\delta_{n2}}{\delta_{n0}-\delta_{n2}}\right)^2 + 1\right] & \delta_{n2} < \delta < \delta_{n0} \end{cases} \tag{3}$$

with the main parameters σ_{max} and δ_{n0}, and two additional shape parameters δ_{n1} and δ_{n2}, which are fixed for all analyses.

In previous publications, e.g. [3, 4], the triaxiality dependence enters the model through a functional dependence of σ_{max} and δ_{n0} using exponential functions. As already mentioned, the identification of this dependence will not be performed by derivation from unit cell simulations obeying porous metal plasticity, but will be fitted to experiments with different stress states ahead of the crack tip. Similar to previous publications, the cohesive strength is calculated based on the function

$$\sigma_{max} = \sigma_\infty \left(1 - \exp\left(\frac{H_{\sigma 1} - H}{H_{\sigma 0}}\right)\right) \tag{4}$$

Therefore, instead of σ_{max}, three parameters, $\sigma_\infty, H_{\sigma 1}$ and $H_{\sigma 0}$have to be determined. In general, the same holds for the critical separation, which reduces with larger triaxiality, so the equation for this is of the form

$$\delta_{n0} = \delta_\infty \left(1 + \exp\left(\frac{H_{\delta 1} - H}{H_{\delta 0}}\right)\right) \tag{5}$$

with again three parameters $\delta_\infty, H_{\delta 1}$ and $H_{\delta 0}$. In general the cohesive energy Γ_{n0}, Eq. 1, using Eqs. 4 and 5 depends on triaxiality, too. However, in the present case it is assumed that changes in Γ_{n0} are of minor importance, since the fracture specimens have a very similar constraint ahead of the crack tip, and for uncracked tensile specimens, the cohesive strength is the dominant para meter; the effect of cohesive energy is negligible. In this investigation the cohesive energy is therefore assumed to be constant, and thus the critical separation is calculated based on a fixed cohesive energy.

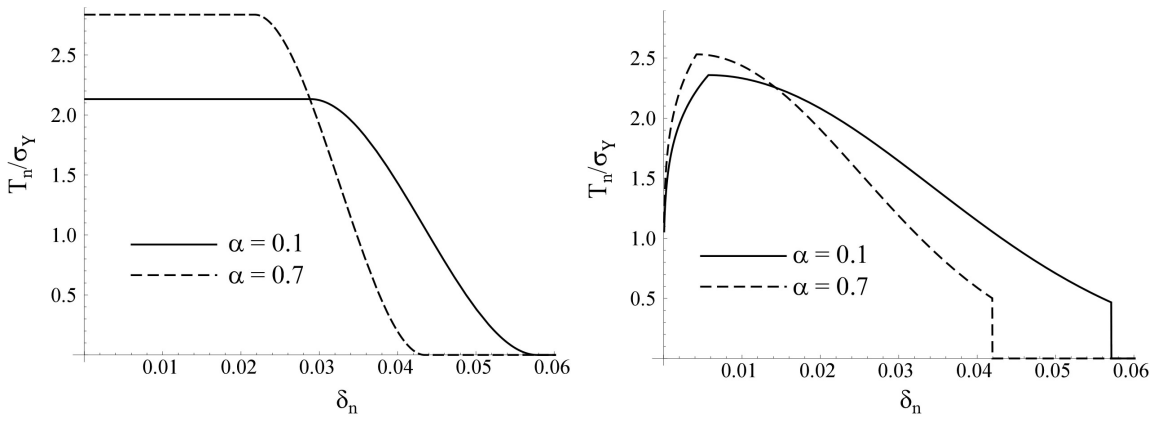

Figure 2: Traction separation laws used in this investigation: (a) proposed in [13], based on two cohesive quantities, σ_{max} and δ_{n0}, Eq. 3, $\delta_{n1}$and δ_{n2}; (b) proposed in [9], derived from plastici ty with strain based failure criterion, Eq. 6.

2.2. Failure strain dependent cohesive model

As already derived in [9], the traction separation law of a cohesive layer with initial width, D, up to attainment of peak stress, σ_{max}, can be established using elastic constitutive relations and deformation plasticity theory, while the softening behaviour can be characterised by an appropriate smooth curve such as the exponential one used in the pr esent work. Taking $\hat{\delta}_n = \delta/D$ as the separation of the bounding surfaces of the process zone normalized by the initial thickness of the process layer, the TSL with three distinct regions of constitutive behaviour is written as:

$$T_n = \begin{cases} \dfrac{2E}{2-\alpha}\hat{\delta}_n & 0 < \hat{\delta}_n \leq \hat{\delta}_{n1} \\ \dfrac{\sigma_y}{\sqrt{\alpha^2-\alpha+1}}\left(\dfrac{2E}{\sigma_y}\dfrac{\sqrt{\alpha^2-\alpha+1}}{2-\alpha}\hat{\delta}_n\right)^n & \hat{\delta}_{n1} \leq \hat{\delta}_n \leq \hat{\delta}_{n2} \\ \sigma_{max}\exp\left[-S\left(\dfrac{\hat{\delta}_n-\hat{\delta}_{n2}}{\hat{\delta}_{n2}}\right)^2\right] & \hat{\delta}_{n2} \leq \hat{\delta}_n \leq 10\hat{\delta}_{n2} \end{cases} \tag{6}$$

The model parameter S in the argument of the exponential function controls the slope of the softening curve. A higher value of S will result in rapid drop of traction beyond its maximum value.

Opposite to the previous approach, the cohesive layer thickness, D, affects the cohesive energy, Γ_{n0}, which in this case is calculated by

$$\Gamma_0 = \int_0^{10\hat{\delta}_{n2}} T_n D d\hat{\delta}_n. \tag{7}$$

Since the fracture resistance, especially the crack initiation, is mainly influenced by Γ_{n0}, D must be treated as additional model parameter. However, since the layer thickness, D, is assumed to be small compared to other geometrical quantities, the actual thickness of the cohesive element may be zero, as usual for the cohesive model.

The value of the peak stress, σ_{max}, is identified based on the failure criterion

$$\varepsilon = Ce^{-1.5H} \tag{8}$$

with C being a material dependent non-dimensional parameter. From this the critical separation $\hat{\delta}_{n2}$ and the maximum stress, σ_{max} are written as

$$\hat{\delta}_{n2} = \frac{2-\alpha}{2}\frac{Ce^{-1.5H_o}}{\sqrt{\alpha^2-\alpha+1}} + \hat{\delta}_{n1}, \tag{9}$$

and

$$\sigma_{max} = T_n|_{\hat{\delta}_n=\hat{\delta}_{n2}} = \frac{\sigma_y}{\sqrt{\alpha^2-\alpha+1}}\left[\frac{2E}{\sigma_y}\frac{\alpha+1}{2-\alpha}Ce^{-1.5H}+1\right]^n \tag{10}$$

Here H is set to a constant value of 0.5, an average value chosen to represent the equivalent plastic strain failure locus for lower triaxilities encountered in plane stress.

2.3. Implementation of triaxiality dependence

The cohesive elements are implemented into the ABAQUS finite element system as user element. While the subroutine used for the Scheider-approach is based on a cohesive element originally developed by Siegmund [3] and extended to various element types and dependencies afterwards, the routine for the Banerjee approach is based on a routine of Gao and Bower [14], modified for the present purpose. Even though the subroutines are completely different, the calculation of triaxiality is realised in the same way for both models using a procedure developed in [7]:

For the first increment the triaxiality value used for the calculation of element stiffness and nodal forces is initialised with some value, for instance 0.333. Subsequently the values are updated after each increment, stored in a common block of the FORTRAN subroutine and used in the following increment. Since the changes in triaxiality are smooth, the error that occurs by taking the stress state of the previous increment is minor.

Another important aspect is the calculation of the actual area of the cohesive interface. Since the implementation is mainly for plane stress or shell elements, where the interface is of line type, the actual thickness of the adjacent continuum element must be transferred to the cohesive element.

This is performed in the same manner as for the triaxiality, i.e. the thickness of the element, which is calculated from ideally plastic conditions (incompressible behaviour) using the available logarithmic strain components by $t = t_0 \left(\exp(-\varepsilon_{11} - \varepsilon_{22})\right)$, is transferred from the continuum element to the adjacent cohesive element via FORTRAN common blocks.

More information about the implementation is written in [4] for the triaxiality dependence and in [15] for the thickness transfer.

3. Experimental data and finite element models

The material used for validation and comparison of the two cohesive approaches is an aluminium alloy Al 5083 [16], which is used in shipbuilding and automotive industry. The thickness of the rolled panels is 3 mm. Various specimens have been manufactured from these panel with and without an initial flaw, namely 20 mm wide tensile specimens with notches of different radii, and fracture mechanics specimens of different sizes. The elastic properties are $E = 70$ GPa and $\nu = 0.33$, and the proof stress is $R_{p0.2} = 242$ MPa, the hardening exponent $n = 0.182$.

The following specimens are used in this article: A centre cracked tensile specimen, M(T), with a total width $2W = 300$ mm, a compact tension specimen, C(T), with a width $W = 50$ mm, and two notched strips with notch radii $R = 2$ mm and $R = 4$ mm. The not ch root width is $W_n = 1/2W = 10$ mm. The structures lead to tri-axialities between 0.35 and 0.55 for the notched bars and well above 0.6 for the precracked specimens. The specimens are shown in Fig. 3.

For quantities that are available from the experiments on fracture specimens: Force, F, remote elongation (v_{LL} for the C(T) specimen and Δl for the M(T)), the crack tip opening displacement, CTOD-δ_5, and the crack extension, Δa. Two curves are generated from these data, the $F(v_{LL})$ curve and the $\delta_5(\Delta a)$ curve, which are then compared to the numerical results. From the notched tensile bar, the force, F, the notch width reduction, Δw, and the remote elongation, Δl are available for comparison.

The finite element mesh is a 2D plane stress model for each geometry. The cohesive elements are always inserted along the symmetry line of the model, where the mesh is severely refined. The length of each cohesive element is 0.125 mm, which has been shown to be sufficient small for mesh independence [17]. For the C(T) specimen, the bolt is modelled by truss elements coupled at

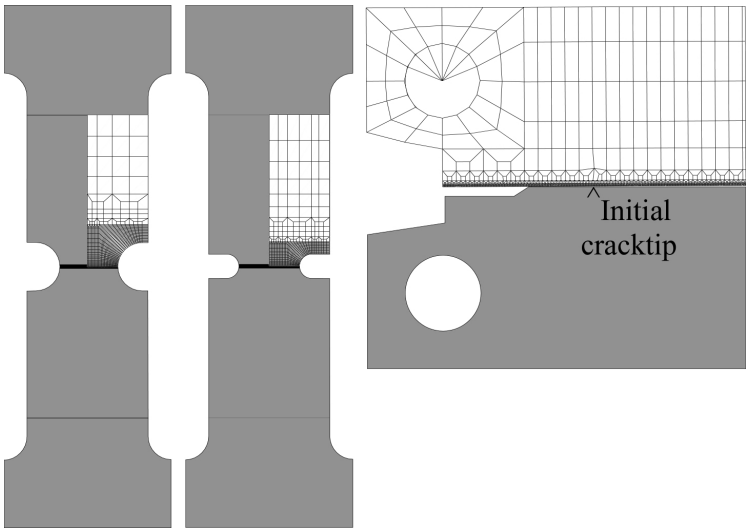

Figure 3: Specimens used in this investigation (all made of sheet material with thickness of 3 mm): two notched strips with notch radius $R = 2$ mm and $R = 4$ mm, respectively, and a C(T) specimen ($W = 50$ mm). The corresponding finite element mesh illustrating the symmetry conditions has been drawn as well.

the centre of the hole, at which a prescribed displacement is applied. For the notched strips, the displacement is appli ed at all top nodes.

4. Results and discussion

4.1. Cohesive model parameters

In a first step the model parameters have to be identified for the respective traction-separation law. In case of the model derived by Banerjee, Eq. 6, this has already been done in [9] based on the C(T) and the notched bar specime n with $R = 2$ mm, leading to $C = 0.6$ and $S = 0.02$; the height of the fracture process zone was set to 0.02 mm. These values are taken for the other specimens, too.

The precracked specimens have also been simulated using the model proposed by Scheider, Eq. 3, but with constant parameters, $\sigma_{max} = 570$ MPa ($\hat{=}2.85\sigma_Y$) and $\Gamma_{n0} = 10$ kJ/m^2. It has been shown in [7], that these parameters are not applicable to uncracked structures, but overpredict the failure strain significantly. In the present study, the three parameters, σ_∞, $H_{\sigma 0}$ and $H_{\sigma 1}$ are identified as follows: The cohesive strength for hight constraint, σ_∞, can be set to the value for precracked specimens, i.e. $\sigma_\infty = 570$ MPa. The other two parameters are adj usted

such that (1) the cohesive strength for low constraint, $H = 0.35$, is equal to the failure stress for the smooth tensile bar ($\sigma_{max}\,|_{H=0.35} = 425$ MPa), and (2) the cohesive strength rises fast to almost its asymptotic value, i.e. $\sigma_{max}\,|_{H=0.45} = 560$ MPa. These boundary values lead to $H_{\sigma 1} = 0.296$ and $H_{\sigma 0} = 0.039$. As already mentioned, the cohesive energy is set constant, and the critical separation δ_{n0} is calculated accordingly. The resulting shapes of the traction-separation curves and the effect of bi-axiality were already shown in Fig. 2 for both approaches. The effect of triaxiality on the cohesive strength according to Eqs. 10 and 4 are sh own in Fig. 4. The influence is somewhat different, especially at higher triaxiality ratios where the cohesive strength for the Banerjee approach decreases, whereas it keeps increasing for the Scheider approach.

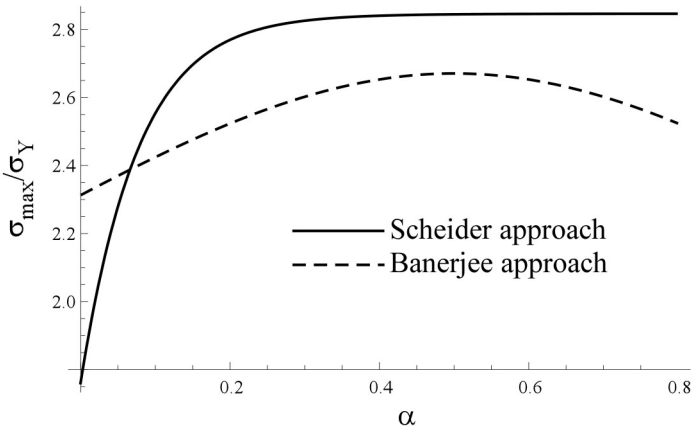

Figure 4: Variation of cohesive strength, σ_{max} on the biaxiality ratio, α.

4.2. Simulation of Aluminium specimens

The comparison for the specimens already presented in [9], namely the notched bar with $R =$ 2 mm and the C(T) specimen are shown in Figs. 5 and 6. It turns out that both models can reproduce the experimental data very wel l. The problem arising from the different constraint conditions is illustrated by showing the simulations with constant parameters, which gives good results for the fracture specimen, but overestimates the experimental failure point of the notched tensile bar severely.

The simulation of the notched tensile bar with larger root radius, $R = 4$ mm, shown in Fig. 7 reveals that the failure points is slightly overestimated by both approaches. However, it must be kept in mind that this simulation is a real predicti on with parameters only fitted to the previous two

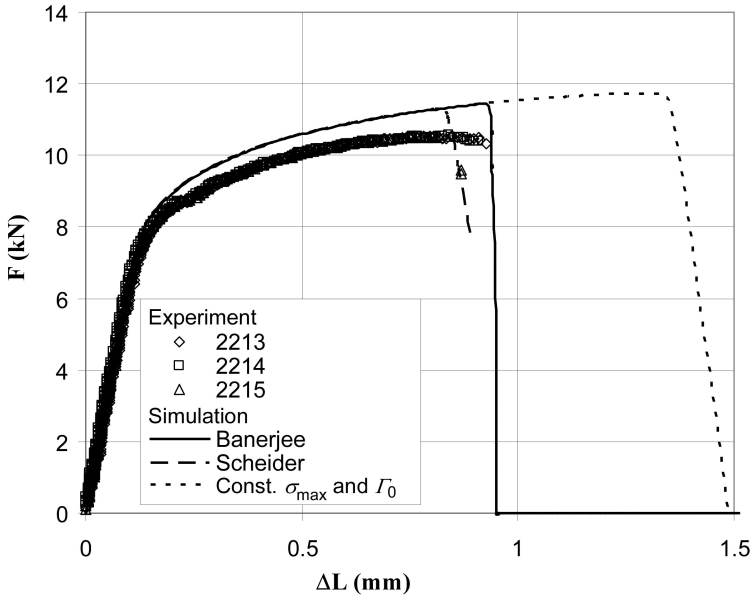

Figure 5: Comparison of the two approaches of cohesive models with respect to reproducing experimental data of a notched tensile bar. Simulation with constant cohesive strength and energy is shown to illustrate the improvement of stress-sta te dependence.

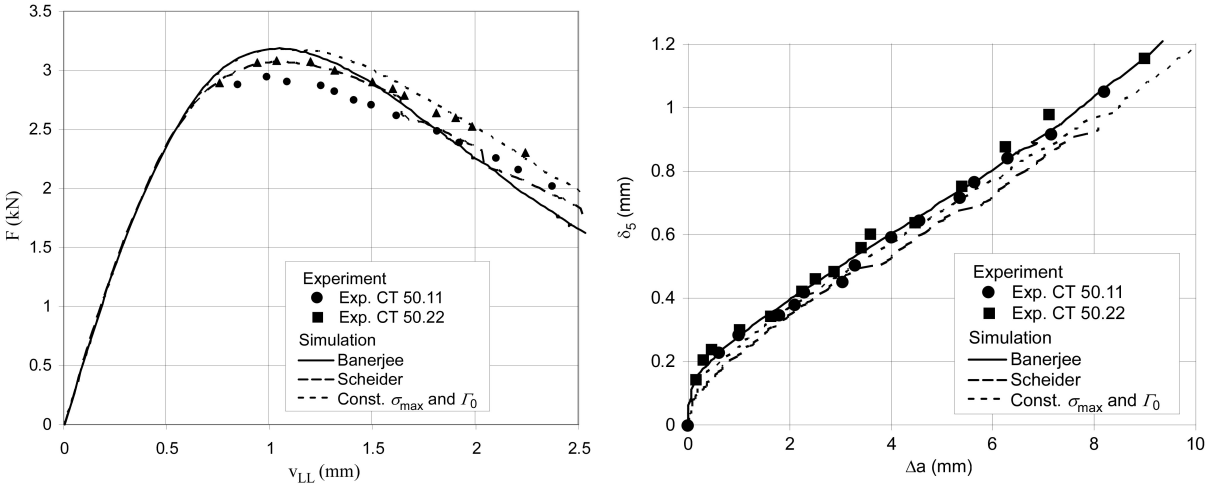

Figure 6: Comparison of both approaches with experimental data of a C(T) specimen. (a) $F(\Delta l)$ curve; (b) $CTOD - \delta_5(\Delta a)$ curve.

experiments. The tendency of increasing remote failure strain with larger notch radius (i.e. reduced constraint) is captured fairly well, and the results of the simulation with constant parameters is agai n much worse. An additional issue visible in Fig. 7 and also in the results of the notched bar with $R = 2$, Fig. 5, is that the deformation behaviour of the simulation has already some difference to the experiment. It is supposed tha t the aluminium cannot exactly be described by the classical isotropic von Mises plasticity, which was used here. A slight anisotropy was observed in the experiments, which is not taken into account. Of course, different stresses affect the failure point of the specimen, thus a small uncertainty in parameter identification is natural.

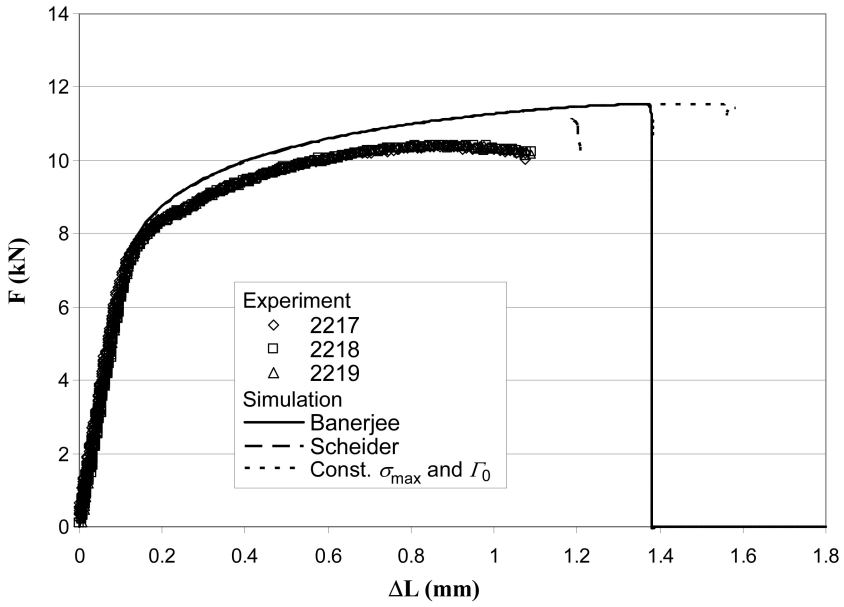

Figure 7: Experiment and simulations of the notched bar with $R = 4$ mm.

The different stress states in cracked and notched specimens can also be illustrated by showing the triaxiality along the line with cohesive elements. For the notched bars the distribution is shown along the notch root just before failure of the specimen, see Fig. 8(a). One can see that the value is always close to 1/3 at the notch, where the transverse stress vanishs (i.e. $\alpha = 0$), whereas the constraint increases towards the center, reaching values which still depend on the notch root ra dius. For the C(T) specimens, the stress triaxiality at the crack tip is higher, see Fig. 8(b). At crack initiation the maximum value is higher than $H = 0.65$, slightly reducing to $H = 0.62$ after some amount of crack extension.

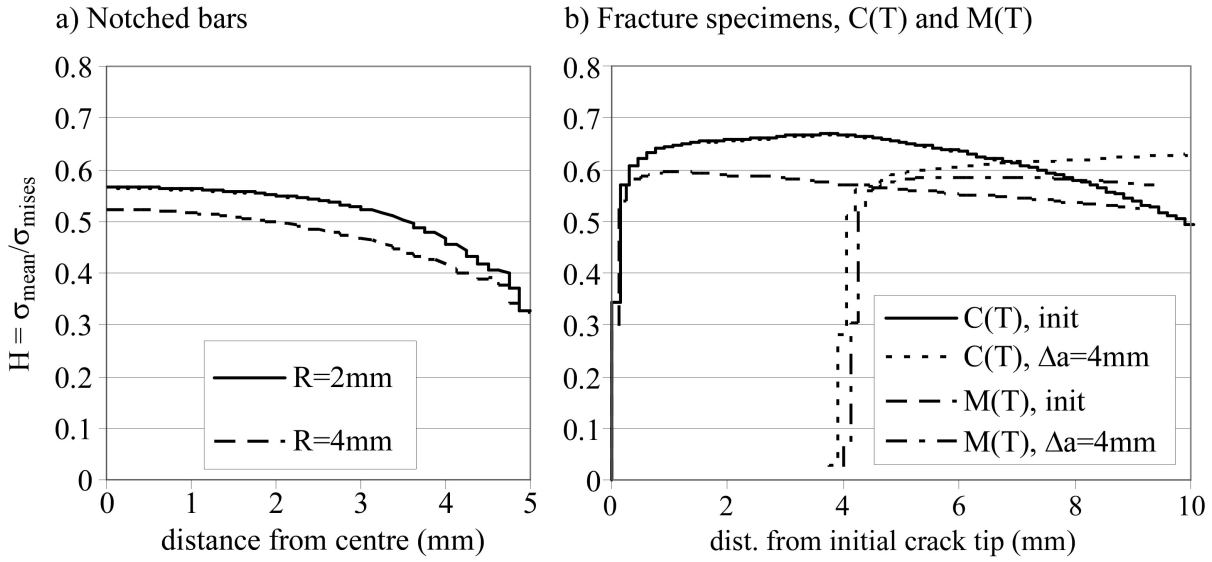

Figure 8: Distribution of triaxiality, H, along the cohesive elements. (a) Notched bars; (b) Ahead of the crack tip of C(T) and M(T) specimens, shown at initiation and after 4 mm crack extension.

Finally, ductile fracture of another specimen is predicted, which has successfully been simulated already in [16] without triaxiality dependent parameters. The M(T) specimen (width $2W$ = 300 mm) investigated here, has a high triaxiality in front o f the crack tip, slightly lower than the C(T) specimen, but not varying much with crack extension, see Fig. 8(b). The residual strength can be predicted with high accuracy with both stress-state dependent approaches, see Fig. 9. Howev er, the slope of the decreasing branch is slightly overestimated, that is the crack extension is too fast compared to the experiment.

5. Conclusions

For the structural assessment of ductile thin-walled structures, it is important to use crack extension models which can cover a wide range of constraint conditions. In the current investigation it has been shown that cracks emanating from stress concentr ations like notches have a significantly different stress-state compared to precracked structures. In order to incorporate the constraint condition into the cohesive model, different approaches have been presented in the literature, two of which have been compared. One model is based on the *classical* traction-separation laws and replaces the parameters cohesive strength and cohesive energy by functions depending on

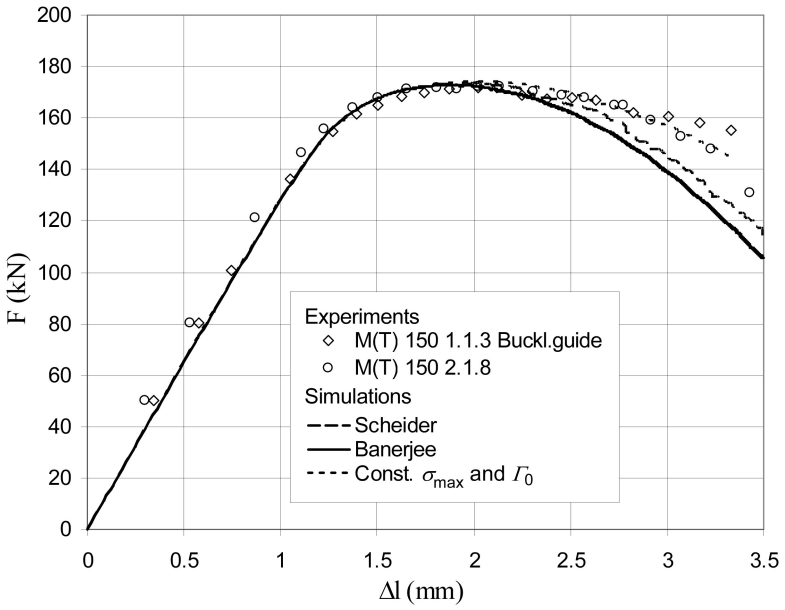

Figure 9: Experiment and simulations of the M(T) specimen ($W = 300$ mm)

triaxiality. The other model under consideration assumes plasticity in the fractur e pocess zone until a (triaxiality dependent) failure strain is reached, and softening occurs. Both approaches have already been implemented into finite element codes, but must be validated before they can be applied to arbitrary thin-walled structures.

The material under investigation was an Aluminium alloy, for which experimental data from notched and precracked specimens was available. It turned out that both models can predict the failure and/or residual strength of all simulated structures fairly we ll. It was also shown that a cohesive model with one constant parameter set is not able to predict both cracked and uncracked bodies at the same time.

Both models have their advantages and their drawbacks. The model based on plasticity in the fracture process zone, throughout the paper denoted as Banerjee-approach) comes along with a very small number of parameters assumed to be material properties: Onl y the failure strain coefficient, C, the assumed width of the fracture process zone, D, and a softening parameter, S, have to be determined. However, the model with the underlying theory can only be applied to plane stress conditions and global mode I fracture (normal separation).

The model incorporating triaxiality dependent cohesive parameters (Scheider-approach) has more parameters to be identified – for the exponential dependency assumed here three coefficients for both the cohesive strength and the cohesive energy must be ide ntified. On the other hand, this model can then be used for arbitrary three-dimensional structures, it is not restricted to a specific stress condition. For other fracture modes, i.e. tangential separation, however, six additional coefficients have to be identified.

The parameter identification was performed in a straight forward manner. The three parameters for the Banerjee-approach could be identified by reproducing the failure point of one notched bar, and the residual strength and crack resistance curve of the C(T) specimen, respectively. Since the triaxiality variation in the C(T) specimen is small and the cohesive energy does not affect the failure point of a notched bar significantly, identification of all six parameters for the Scheider-approach was not possible. Therefore, the cohesiv e energy was assumed to be constant, instead, with a small value identified in a previous publication for high constraint conditions. The three remaining parameters were identified based on the high constraint cohesive strength, which can be fitted to the C(T) specimen, the failure stress for the smooth tensile bar having a small triaxiality value of $H = 0.33$ and only one fit-parameter left to adjust. These simple methods were sufficient to achieve the results presented.

6. Acknowledgment

The authors would like to acknowledge the support provided by ISRO-IITM cell grant no. ICSR/ISRO-IITM/APM/08-09/124/ANUR for the work carried out at IIT Madras.

References

[1] T. Pardoen, F. Hachez, B. Machioni, P.H. Plyth and A.G. Atkins. Mode I fracture of sheet metal. J Mech Phys Solids 52 (2004) 423-452.

[2] U. Zerbst, M. Heinimann, C. Dalle Donne and D. Steglich. Fracture and damage mechanics modelling of thin-walled structures An overview. Engng Fract Mech 76 (2009) 5-43.

[3] T. Siegmund and W. Brocks. A numerical study on the correlation between the work of separation and the dissipation rate in ductile fracture. Engng Fract Mech 67 (2000) 139-154.

[4] M. Anvari, I. Scheider and C. Thaulow. Simulation of dynamic ductile growth using strain-rate and triaxiality dependent cohesive elements. Engng Fract Mech 73 (2006) 2210-2228.

[5] I. Scheider. Derivation of separation laws for cohesive models in the course of ductile fracture. Engng Fract Mech 76 (2009) 1450-1459

[6] T. Pardoen and J.W. Hutchinson. An extended model for void growth and coalescence. J Mech Phys Solids 48 (2000) 24672512.

[7] I. Scheider and W. Brocks: Effect of cohesive law and triaxiality dependence of cohesive parameters in ductile tearing. In: Fracture of Nano and Engineering Materials and Structures, edited by E.E. Gdoutos, Springer; Dordrecht, The Netherlands (2006).

[8] A. Banerjee and R. Manivasagam. Triaxiality dependent cohesive zone model. Engng Fract Mech 76 (2008) 1761-1770.

[9] M. Rajendran, I. Scheider and A. Banerjee, Stress state dependent cohesive zone model for thin walled structures. Key Engng Mater 417-418 (2010) 353-356.

[10] J.L. Chaboche, R. Girard and P. Levasseur, On the interface debonding models. Int. J Damage Mech. 6 (1997) 220-257.

[11] I. Scheider and W. Brocks, The effect of the traction separation law on the results of cohesive zone crack propagation analyses. Key Engng Mater 251-252 (2003) 313-318.

[12] C. Fan, P.-Y. Ben Jar, J.J.R. Cheng, Cohesive zone with continuum damage properties for simulation of delamination development in fibre composites and failure of adhesive joints. Eng. Fract. Mech. 75 (2008) 3866-3880.

[13] I. Scheider and W. Brocks, Simulation of cup-cone fracture using the cohesive model. Engng Fract Mech 70 (2003) 1943-1961.

[14] Y.F. Gao and A.F. Bower, A simple technique for avoiding convergence problems in finite element simulations of crack nucleation and growth on cohesive interfaces. Modeling Simul. Mater. Sci. Engng. 12 (2004) 453-463.

[15] I. Scheider and W. Brocks, Cohesive elements for thin-walled structures, Comp Mater Sci 37 (2006) 101-109.

[16] I. Scheider, M. Schödel, W. Brocks and W. Schönfeld. Crack propagation analyses with CTOA and cohesive model: Comparison and experimental validation. Engng Fract Mech 73 (2006) 252-263.

[17] I. Scheider, W. Brocks and M. Schödel. Simulation of crack extension in shell structures and prediction of residual strength. Arch Appl Mech 76 (2006) 655-665.